Short-range order and precipitation in Fe-rich Fe-Cr alloys: Atomistic off-lattice Monte Carlo simulations

Paul Erhart,* Alfredo Caro, Magdalena Serrano de Caro, and Babak Sadigh
Chemistry, Materials, Earth, and Life Sciences Directorate, L-367, Lawrence Livermore National Laboratory, Livermore, California, 94550, USA

(Received 24 July 2007; revised manuscript received 17 December 2007; published 21 April 2008)

Short-range order (SRO) in Fe-rich Fe-Cr alloys is investigated by means of atomistic off-lattice Monte Carlo simulations in the semi-grand-canonical ensemble using classical interatomic potentials. The SRO parameter defined by Cowley [Phys. Rev. **77**, 669 (1950)] is used to quantify the degree of ordering. In agreement with experiments a strong ordering tendency in the Cr distribution at low Cr concentrations ($\lesssim 5\%$) is observed, as manifested in negative values of the SRO parameters. For intermediate Cr concentrations ($5\% \lesssim c_{\mathrm{Cr}} \lesssim 15\%$), the SRO parameter for the α phase goes through a minimum, but at the solubility limit, the α-phase still displays a rather strong SRO. In thermodynamic equilibrium for concentrations within the two-phase region the SRO parameter measured *over the entire* sample therefore comprises the contributions from both the α and α' phases. If both of these contributions are taken into account, it is possible to quantitatively reproduce the experimental results and interpret their physical implications. It is thereby shown that the inversion of the SRO observed experimentally is due to the formation of stable (supercritical) α' precipitates. It is not related to the loss of SRO in the α phase or to the presence of unstable (subcritical) Cr precipitates in the α phase.

DOI: 10.1103/PhysRevB.77.134206 PACS number(s): 61.43.Dq, 82.60.Lf, 81.30.Mh, 02.70.Uu

I. INTRODUCTION

Iron-chromium steels are of great technological importance due to their superior properties at high temperatures and under aggressive chemical conditions. In particular, they are used in reactor environments because of their good swelling and corrosion resistance.[1,2] The precise origin of many of these beneficial features is still uncertain. Creep resistance is customarily associated with the presence of *small* α' precipitates, while embrittlement has been related to the presence of *larger* α' precipitates. The α and α' phases are the Fe-rich and Cr-rich solid solutions into which the body-centered cubic (bcc) phase of the alloy decomposes at temperatures below about 1000 K. At yet higher temperatures, a third phase appears around equiatomic composition, known as the σ phase.

The phase diagram for this alloy has been assessed using the CALPHAD methodology.[3,4] In this approach, the alloy was assumed to behave as a subregular solution at temperatures below the existence range of the σ phase. In other words, the heat of formation is assumed to be positive over the entire composition and it is parameterized by a second degree polynomial in the Redlich-Kister expansion. There is, however, an ensemble of experimental observations at relatively low temperatures in both annealed and irradiated samples, which suggest a more complex behavior.[5–7]

A breakthrough in the understanding of the microstructure of these alloys was made through neutron diffraction measurements,[8] which showed (1) negative Cowley short-range order (SRO) parameters [see Eq. (1) below] at small Cr concentrations indicating strong short-range ordering of Cr atoms and (2) an inversion of the sign of these parameters with increasing Cr concentration, which seems to imply a change of SRO in the solid solution as it approaches the solubility limit. The implications of these discoveries for the interpretation of creep resistance and embrittlement are apparent since SRO is known to affect the mobility of dislocations[9] and precipitation plays a role in intergranular cracking.[10]

Nonetheless, the understanding of the atomistic details of the complex behavior of this alloy is still incomplete. This situation has motivated a number of recent first-principles studies,[11–15] which addressed the energetics of this system. These calculations revealed a change of sign in the heat of formation of the solution from the negative to the positive side as the Cr concentration increases above approximately 10%.[11–15] Detailed analysis of the origin of this anomaly showed that, while the heat of solution of a Cr impurity in Fe is large and negative, magnetic frustration leads to a strong Cr-Cr repulsion, causing the heat of formation to assume large positive values as the Cr content increases.

These advances in the understanding of the energetics of Fe-Cr alloys have provided the basis for the development of accurate interatomic potential models, which enable large scale simulations of the microstructural evolution. Two approaches were developed, known as the two band model[16] and the composition dependent model,[17] which both address the complex shape of the heat of formation curve at 0 K as determined from the aforementioned first-principles calculations. A third approach[18] to model the finite temperature properties of this alloy is based on a cluster expansion fitted to density functional theory data, which is then used in combination with lattice Monte Carlo simulations to study precipitation and ordering. By using the composition dependent model, we recently studied the implications of the change in sign of the heat of formation on the thermodynamic behavior at finite temperatures and proposed a modified phase diagram for Fe-Cr in the region of low Cr content and temperatures below the range of existence of the σ phase.[19] In fact, compared to the CALPHAD assessment,[4] which is based on

the assumption of a *standard segregating binary* mixture (positive heat of mixing at all concentrations, compare above), a better agreement with the experimental location of the *solvus* was obtained.

From our viewpoint, three aspects render the study of SRO in Fe-Cr alloys particularly interesting: (1) Experimental measurements of SRO parameters of heterogeneous systems (such as mixtures of the α and α' phases) provide only compound quantities equivalent to averages over the entire sample. (2) In Fe-Cr, this situation is further complicated by the ordering tendency of the system at low Cr concentrations. (3) The recent advances in the development of Fe-Cr interatomic potentials and the availability of suitable simulation techniques provide the possibility to explore the atomistic details of these processes. Thereby, we are able to resolve the contributions to the experimentally measured quantities and understand the microscopic behavior of the material. We discuss the evolution of the SRO parameter in a mixture of two phases and the evolution of the SRO parameter upon coarsening, induced, e.g., by aging or irradiation. It is shown that the experimentally observed inversion of the SRO parameter is due to the formation of stable (supercritical) α' precipitates. It is not related to an overall loss of SRO, to a loss of SRO in the α phase, or to the presence of unstable (subcritical) Cr precipitates in the α phase. Furthermore, by using the same order parameter as in the experimental reports, we reconcile an apparent discrepancy between experimental data and the model predictions reported in Ref. 17.

The paper is organized as follows. Section II introduces the order parameters used in this work, while Sec. III describes the methodology. Section IV contains the results of the simulations organized into three subsections, which address (i) the relation between the chemical potential difference and the concentration, (ii) the SRO in the α phase, and (iii) the evolution of the SRO in the two-phase region. In Sec. V, a simple expression for the SRO in the two-phase region is introduced, which is subsequently employed to interpret the experimental result and to derive the temperature dependence of the SRO parameter. Section VI summarizes the conclusions.

II. MEASURES OF SHORT-RANGE ORDER

Short-range order in binary alloys is conveniently measured by means of the order parameter introduced by Cowley,[20] which has been widely applied in the past (see e.g., Refs. 8, 21, and 22). The SRO parameter for the kth shell of a Cr atom is defined as

$$\alpha_{\mathrm{Cr}}^{(k)} = 1 - \frac{Z_{\mathrm{Fe}}^{(k)}}{Z_{\mathrm{tot}}^{(k)}(1 - c_{\mathrm{Cr}})}, \tag{1}$$

where $Z_{\mathrm{Fe}}^{(k)}$ denotes the number of Fe atoms in the kth shell, $Z_{\mathrm{tot}}^{(k)}$ is the total number of atoms in the same shell, and c_{Cr} is the overall (total) Cr concentration. It is instructive to consider several special cases: (1) If a Cr atom is exclusively surrounded by other Cr atoms, $Z_{\mathrm{Fe}}^{(k)}=0$ and $\alpha_{\mathrm{Cr}}^{(k)}=1$. (2) If one has a completely random distribution, the ratio $Z_{\mathrm{Fe}}^{(k)}/Z_{\mathrm{tot}}^{(k)}$ equals $c_{\mathrm{Fe}}=1-c_{\mathrm{Cr}}$ and $\alpha_{\mathrm{Cr}}^{(k)}=0$. (3) Finally, if each Cr atom is surrounded exclusively by Fe atoms $Z_{\mathrm{Fe}}^{(k)}=Z_{\mathrm{tot}}^{(k)}$ and therefore

$$\alpha_{\mathrm{Cr}}^{(k)} = -\frac{c_{\mathrm{Cr}}}{1 - c_{\mathrm{Cr}}}, \tag{2}$$

which provides a lower bound to the SRO parameter; in other words, it indicates the maximum possible degree of short-range order at a given composition.

Previous experimental studies of SRO in Fe-Cr have used a SRO parameter specific for the bcc lattice.[8] This parameter is defined as a coordination number-weighted average of the SRO parameters defined above for the first and second neighbor shells,

$$\beta = \frac{8\alpha_{\mathrm{Cr}}^{(1)} + 6\alpha_{\mathrm{Cr}}^{(2)}}{14}. \tag{3}$$

Other studies[22] assumed the SRO parameters $\alpha_{\mathrm{Cr}}^{(1)}$ and $\alpha_{\mathrm{Cr}}^{(2)}$ to be the same which leads to similar results. For consistency with the literature and to simplify comparison, we focus on this bcc-specific weighted SRO parameter in the following sections. In Sec. IV B, we will, however, explicitly discuss the SRO parameters for different shells, which yields insights into the range of Cr-Cr interactions.

III. METHODOLOGY

A. Algorithm

If one is to study the problem of short-range order and the formation of precipitates in a segregating alloy while including the effects of local relaxations, one requires an algorithm, which is capable of efficiently taking into account both chemical mixing and atomic relaxation. The former can be achieved by employing a Monte Carlo (MC) algorithm, which allows changes in the chemical identity of the particles, as will be discussed in the following two paragraphs. In principle, atomic relaxations can be captured by a displacement MC algorithm but for the problem at hand molecular dynamics (MD) simulations turn out to be more efficient. The basic approach is thus to alternate MC moves and MD steps.

The usual approach to model the effects of chemical mixing in heterogeneous solid solutions is to employ a MC swap algorithm, in which the global composition is kept constant and the system is advanced by swapping pairs of particles of different chemical identities. The change in total energy is employed to decide whether a move is accepted or rejected. For single phase systems one can also use a semi-grand-canonical ensemble (SGC), in which the composition is determined by the difference of the chemical potentials $\Delta\mu$ of the species, and each MC move is equivalent to exchanging particles with the external reservoirs of both chemical species. Unlike the swap scheme the SGC-MC algorithm can be formulated to operate only on one particle at a time. Therefore, the latter can be more easily parallelized.

Within a two-phase region of the phase diagram the relation between the concentration c and the chemical potential difference $\Delta\mu$ has an infinite slope. In principle, the SGC-MC algorithm cannot deal with such situations, and in

order to keep the global composition within the miscibility gap, one must apply an additional constraint. The latter can be formally derived as a constraint on the concentration fluctuations, the formal derivation of which will be given elsewhere.[23] For the present study, we implemented the constraint in a very simple way, namely, as a limitation on the number of particles in the reservoirs: When the (externally specified) maximum global concentration of solute atoms is reached, MC moves which lead to a further increase in the solute concentration are always rejected, regardless of their energy, i.e., the maximum number of solute atoms is limited. To clarify this approach, consider the case in which constraints are imposed on both the maximum and the minimum number of solute atoms. In the (hypothetical) limit that the difference between the lower and upper limit vanishes, this algorithm would become equivalent to the swapping algorithm. We recall here that the primary motivation behind the development of this algorithm is that it can efficiently be parallelized.

To summarize, for values of $\Delta\mu$ within the α phase, our simulations start with pure Fe samples and by alternating MC moves with MD steps the sample loads solute atoms and relaxes the lattice in the solid solution until the equilibrium composition is reached and stationary fluctuations reach canonical values. If $\Delta\mu$ exceeds the stability range of the α phase, the simulation still starts from a pure Fe sample and first establishes a solid solution in the α phase. Since the formation of a supercritical nucleus is linked to a nucleation barrier, precipitation does not occur immediately but only after some residence time. The system therefore evolves initially in a single phase. However, as soon as the spatial fluctuations in the composition have led to the formation of supercritical nuclei, they will grow rapidly and the global Cr concentration rises sharply. When the target global composition is reached, or equivalently, when the volume fraction of α' precipitates reaches the target value, the concentration constraint keeps the system fluctuating around the preset global composition, and coarsening of the precipitates is observed. The residence time prior to the formation of stable α' precipitates depends on $\Delta\mu$, i.e., on the chemical driving force for precipitation. If the difference of the chemical potentials exceeds the stability range of the α phase only slightly, residence times are rather long (in terms of MC steps) and meaningful averages (with regard to SRO) can be obtained (see Fig. 4 below for an example).

As described above, in the early stages of a simulation, some α' nuclei may exist in the α phase, but they do not yet exceed the critical size. Fluctuations in the composition eventually lead to the formation of stable (supercritical) α' precipitates, which subsequently coarsen. While this evolution cannot be related to a physical time scale because atoms do not move via diffusion but via swaps, it nevertheless represents the sequence of steps followed during the real evolution of a saturated α phase. Similarly, SRO develops in the α phase in the course of the simulation and reaches equilibrium before the α/α' microstructure emerges, reflecting the fact that precipitation is a first order phase transition with a nucleation barrier, while order-disorder is not.

B. Computational details

We used samples with $40\times40\times40$ conventional bcc unit cells equivalent to 128 000 atoms. Simulations were carried out for temperatures between 100 and 900 K and chemical potential differences between −0.45 and 0.12 eV/atom. To obtain the data presented below, the samples were run for a total of 3×10^3 MC steps/atom. We have found this number to be sufficient to obtain well converged results for the SRO parameter. For chemical potential differences which are equivalent to Cr concentrations below the solubility limit, the system quickly equilibrates. Averages are obtained over all configurations in the Markov chain after the initial equilibration period. For values of the chemical potential difference which correspond to concentrations slightly *above* the solubility limit, the system does not immediately separate into two phases due to the nucleation barrier associated with this process (compare previous paragraph). Instead, one observes a transient state during which the system equilibrates in the solid solution. Once a supercritical nucleus of the secondary phase has formed, it grows very quickly and the system decomposes into two phases. (An example of this behavior is shown in Fig. 4 below.) The existence of this transient regime allows us to obtain meaningful averages for concentrations slightly inside the miscibility gap corresponding to oversaturated solid solutions. (In Fig. 4, this is the case for the first 1000 MC steps.) All of the data presented in the following sections (specifically the data shown in Figs. 2 and 3) were obtained in this manner, i.e., as averages over configurations which correspond to the α-phase only. A detailed description of a simulation which develops from a single to a two-phase system and which illustrates the transient behavior referred to above is given in Sec. IV C.

The interatomic potential used in this work is taken from Ref. 19. It is an embedded atom method type potential based on the Fe potential by Mendelev *et al.*[24] and the Cr potential by Wallenius *et al.*[25] To model the Fe-Cr alloy, the potential for the mixed interaction has been constructed to exactly reproduce the mixing enthalpy curve obtained from first-principles calculations.[12]

IV. RESULTS

A. Chemical potential difference vs concentration

Figure 1 shows the relation between the equilibrium Cr concentration c_{Cr} and the difference of the chemical potentials $\Delta\mu=\mu_{\mathrm{Cr}}-\mu_{\mathrm{Fe}}$ for different temperatures. It is found that the dependence cannot be reproduced by using the expression for an ideal solution, $\Delta\mu=\Delta\mu^0+k_BT\ln c_{\mathrm{Cr}}/(1-c_{\mathrm{Cr}})$. The curves can, however, be reasonably well fit assuming a regular solution,[26]

$$\Delta\mu=\Delta\mu^0+\Omega(1-2c_{\mathrm{Cr}})+k_BT\ln\frac{c_{\mathrm{Cr}}}{1-c_{\mathrm{Cr}}}, \tag{4}$$

as shown by the lines in Fig. 1, where $\Delta\mu^0$ and Ω were treated as the fitting parameters.

B. Short-range ordering in the α phase

The results for the bcc SRO parameter β defined in Eq. (3) are shown in Fig. 2. Several observations can be made:

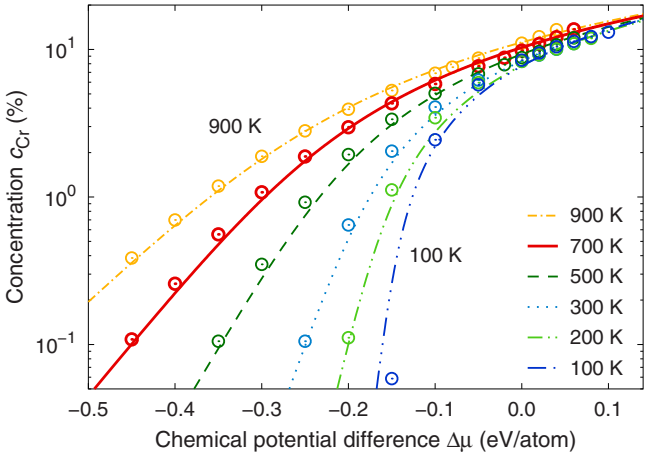

FIG. 1. (Color online) Relation between chemical potential difference and Cr concentration in α-Fe. The data points were obtained by simulation. The lines are fits to Eq. (4).

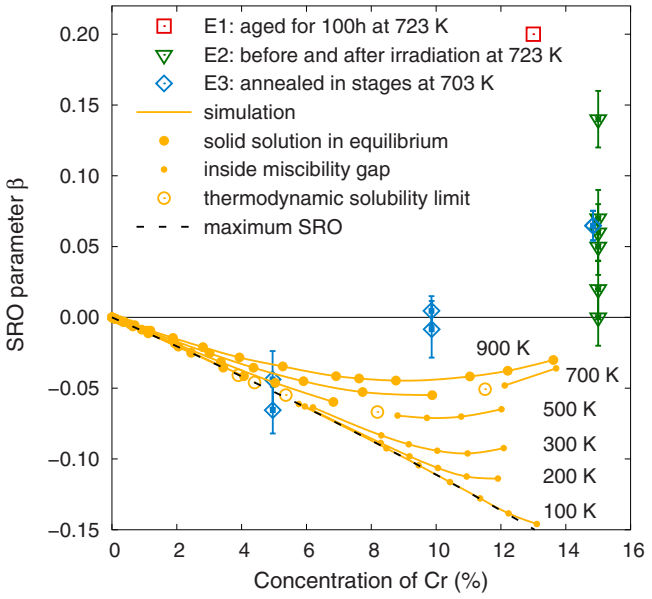

FIG. 2. (Color online) Dependence of the short-range order parameter β, defined by Eq. (3) on the total Cr concentration. The circles show simulation data. The solid lines serve as guides to the eyes. The dashed line represents the maximum possible order as given by Eq. (2). The solubility limits for each temperature, which are indicated by the open circles, were taken from Ref. 19. The points which belong to concentrations beyond these limits, i.e., inside the miscibility gap, are indicated by small filled circles. They have been obtained by averaging over configurations of the transient single phase system (oversaturated solid solution) which is observed prior to nucleation of the α' phase (compare Sec. III B). E1: experimental data from Ref. 21, E2: experimental data from Ref. 22, and E3: experimental data from Ref. 8.

At small concentrations β becomes more negative with increasing Cr concentration. At low temperature, the curves approach the theoretical lower limit for the SRO parameter (dashed line in Fig. 2) given by Eq. (2). For larger concentrations the SRO parameter increases, showing a minimum between 8% and 12% Cr, the location of which is only weakly dependent on temperature. We conclude that in the entire compositional range where only the α phase exists, its SRO is strong. Furthermore, we conclude that the absolute value of the SRO versus composition has a maximum at around 10% Cr, quite independent of composition.

The minimum in the curves occurs due to the onset of a saturation of the Cr distribution: Since the interaction energy between two Cr atoms in Fe is large and positive,[27] the lowest energy configurations maximize the separation between the Cr atoms. This is the source of the ordering tendency in this system which attempts to maximize the number of nonalike neighbors, i.e. $Z_{\mathrm{Fe}}^{(k)}/Z_{\mathrm{tot}}^{(k)}$ in Eq. (1) approaches one.

As the Cr concentration increases, the fraction of configurations which maximize the Cr-Cr separation decreases. At the same time, the entropy gained by randomizing the system increases significantly since the total number of possible configurations rapidly increases. The SRO is therefore both strongly temperature and concentration dependent. In the limit of zero temperature, i.e., in the absence of entropic effects, the SRO parameter β approaches its lower bound given by Eq. (2). At high temperatures, it becomes less negative since the entropy favors randomization of the system. As the Cr concentration increases, the entropy gained by randomization eventually exceeds the energy gained by ordering causing the minimum in the SRO parameter curves.

This effect is further illustrated in Fig. 3 which shows the SRO parameters $\alpha_{\mathrm{Cr}}^{(k)}$ for the first three neighbor shells. For the first shell, the calculated SRO parameter at low temperatures closely follows the theoretical limit [Eq. (2)] corresponding to a situation in which the first shell around any Cr atom is exclusively filled with Fe atoms. With increasing temperature the point at which the SRO parameter, $\alpha_{\mathrm{Cr}}^{(1)}$, deviates from the theoretical limit is shifted toward smaller concentrations. For the second and third shells, this deviation occurs at yet lower temperatures and concentrations. This behavior is correlated with the interaction energy vs separation curves given in Ref. 27 which show a significant drop of the Cr repulsion energy with separation.

As mentioned above the SRO parameter β for larger Cr concentrations becomes less negative with increasing temperature. However, for the interaction model used in the present work it does not become zero before melting, which would indicate a completely random solution. It should be pointed out that this observation is a property of this model and is not necessarily related to the behavior of the real alloy, which undergoes both magnetic and structural transitions (ferromagnetic-paramagnetic, $\alpha-\gamma-\delta$) before melting, transitions that are not described by the present empirical potential.

Figure 2 includes several experimental data points.[28] They indicate a transition of the SRO parameter through a minimum and subsequently an increase up to positive values. The occurrence of a minimum is seemingly similar to the simulation results but the two minima have different physical origins: The experimentally determined SRO represents an average over the entire sample, eventually including both the α phase and α' precipitates. In contrast, the simulation data shown in Fig. 2 have been explicitly obtained for the α-phase only (compare Sec. III B) and the occurrence of a minimum is an intrinsic property of this solid solution (as discussed

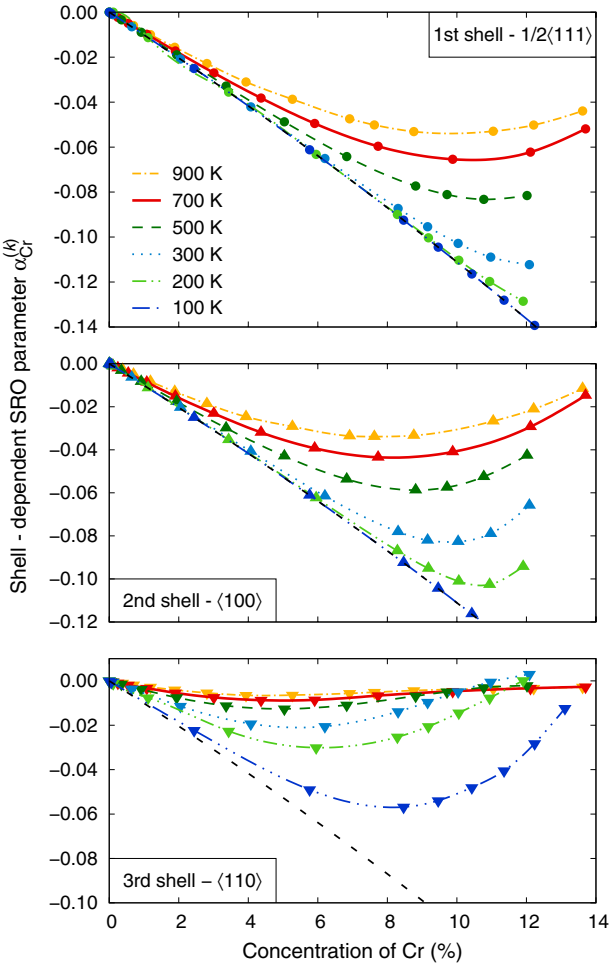

FIG. 3. (Color online) Short-range order parameters for the first three neighbor shells, as defined in Eq. (1). The SRO parameter displays a minimum as a function of Cr content and becomes less negative with increasing temperature. The latter effect is the more pronounced the larger the shell radius. The dashed line shows the lower bound for the SRO order given by Eq. (2)

above). Thus, in order to explain the relation between the experimentally measured SRO which involves the entire sample and its values in the α and α' phases, we must first understand the contribution of the α' precipitates to the measured SRO parameter.

C. Bimodal distribution of the short-range order parameters in the two-phase region

In order to illustrate the contributions of the α phase and α' precipitates to the SRO parameter, we consider one particular simulation (T=500 K, $\Delta\mu$=0.06 eV/atom). At this temperature, the chemical potential difference chosen implies that without constraints on the total concentration, the system in equilibrium would be in the α' phase, whereas the constraint keeps the system inside the two-phase region. This particular simulation is suitable for illustrating the transition from a single to a two-phase system during the course of the MC simulation: The initial sample contains Fe atoms only and the SRO parameter β measured over the entire sample is

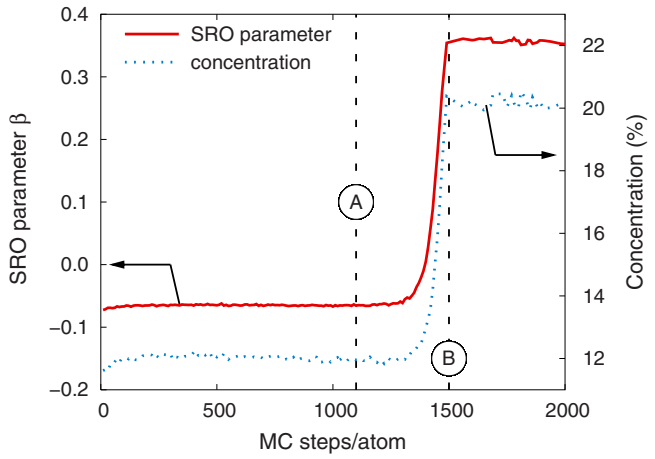

FIG. 4. (Color online) Evolution of the average concentration and SRO parameter during the course of a simulation (T=500 K, $\Delta\mu$=0.06 eV/atom). The points A and B refer to the configurations shown in Figs. 5 and 6.

zero. During the very first steps of the simulation, the number of Cr atoms sharply increases. Already after about 200 MC steps/atom, the concentration of Cr settles to a value of about 12% and the SRO parameter β adopts a value of about −0.07, as shown in Fig. 4. In this stage, the entire sample is an Fe-rich saturated homogeneous solid solution.

Figure 5 shows histograms of the number distribution of SRO parameters obtained by averaging over every Cr atom in the sample after 1100 MC steps per atom (point A in Fig. 4) which is a representative configuration for the Fe-rich homogeneous solid solution (pure α phase). There is one pronounced peak on the negative side equivalent to the SRO of the α phase. Note that the range of SRO parameters also includes some positive values. This is related to the saturation of the α phase, which in equilibrium at this temperature has a solubility of about 8% Cr,[19] and to the formation of unstable (subcritically sized) α' nuclei. For further illustra-

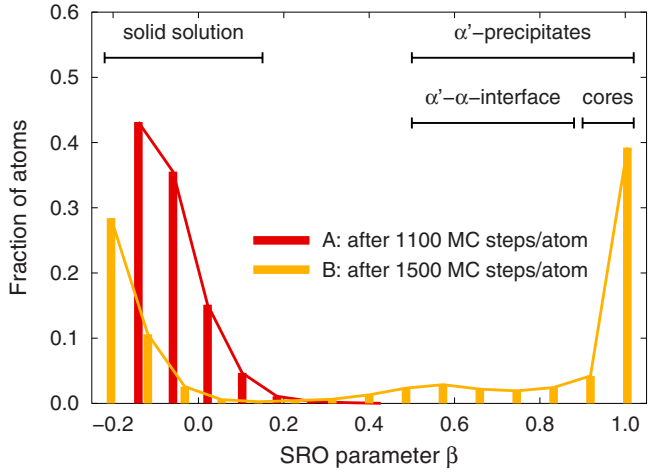

FIG. 5. (Color online) Number distribution of SRO parameter before (A) and after (B) the formation of supercritically sized α' precipitates. The corresponding configurations are shown in Fig. 6. The simulation was carried out at 500 K using a chemical potential difference of $\Delta\mu$=0.06 eV/atom.

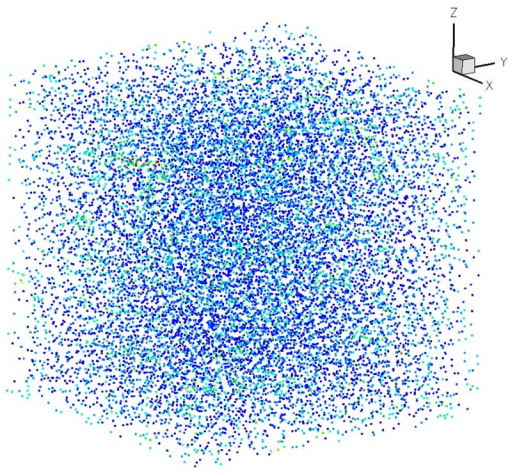

(a) configuration A: after 1100 MC steps/atom

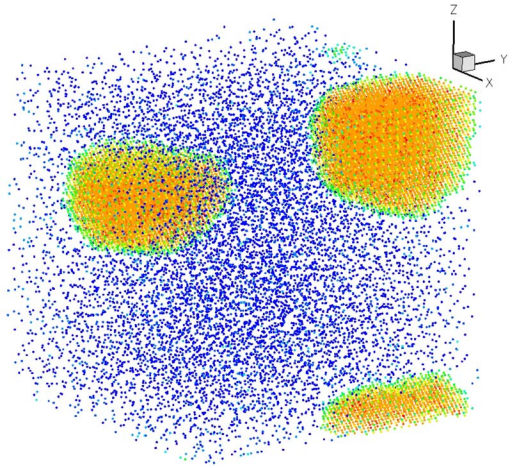

(b) configuration B: after 1500 MC steps/atom

FIG. 6. (Color online) Atomic configurations before (a) and after (b) the formation of supercritical α' precipitates. Only Cr atoms are shown with a color coding based on their SRO parameter: blue/green (dark gray)—negative or small positive SRO parameter (Fe-rich solid solution, α phase) and yellow/red (light gray)—positive SRO parameter (α' precipitates, α/α' interface). The simulation was carried out at 500 K using a chemical potential difference of $\Delta\mu=0.06$ eV/atom.

tion, the configuration is shown in Fig. 6(a), clearly indicating the absence of precipitation.

The system remains in this metastable state up to about 1300 MC steps per atom. Then, it undergoes a rapid transition, as indicated both by the SRO parameter (average over the entire sample) and the concentration. At this point, supercritically sized α' precipitates have formed which subsequently grow. Without constraints their size would increase until the *total* concentration of Fe reaches the value corresponding to the given chemical potential difference on the Cr-rich side of the phase diagram. The final Fe concentration will therefore assume some value lower than the solubility of Fe in Cr. In the present simulations, the Cr concentration is, however, enforced to be about 20% or lower. The distribution of SRO parameters shown after 1500 MC steps/atom (point B in Fig. 4) in Fig. 5 now clearly displays two distinct peaks which result from the α phase ($\beta \lesssim 0.2$) and the α' precipitates ($\beta \approx 1$), respectively (compare Sec. V).

The resulting SRO parameter averaged over the entire sample is about 0.35. Note that the SRO parameter of the Cr atoms in the α phase drops after the occurrence of α' precipitates. This is mostly due to the higher global Cr concentration which enters in Eq. (1). It is therefore an effect of the concentration dependence entering the definition of the SRO parameter, not an indication for an actual higher degree of order in the α phase. At the same time, the concentration of Cr in the α phase returns to the solubility limit. This behavior corresponds to the curves in Fig. 2. The atomic configuration after 1500 MC steps/atom is visualized in Fig. 6(b), which clearly shows the formation of precipitates and the emergence of a two-phase mixture. The color scale furthermore illustrates the intermediate SRO parameter obtained for atoms at the α/α' interface.

This example clearly illustrates the transition from an Fe-rich saturated solid solution to a two-phase system. It demonstrates how in this range of Cr concentrations the local SRO parameter can be used to identify atoms as being either part of the α or α' phase [see in particular Fig. 6(b)]. Furthermore, it elucidates the different contributions which lead to a given measurable SRO parameter and how the latter can be utilized to detect the formation of α' precipitates. In the following section, these observations will be generalized and combined to obtain a general expression for the average SRO parameter as a function of Cr concentration.

V. DISCUSSION

A. Interpretation of the short-range order inversion

The results presented above demonstrate that particular care must be exercised when interpreting the SRO parameter in the case of a two-phase mixture. In the following, we focus on the case of a Fe-rich Fe-Cr alloy at low temperature.

While the SRO parameter for Cr atoms in the α phase is typically small and negative, the SRO parameter for Cr atoms in the α' phase is close to 1. Since experimentally the SRO is obtained over the entire sample, the measured value is an average over all types of local short-range order. This average is the weighted sum of the contributions from the α and α' phases as well as the α/α' interface. However, for simplicity, in what follows, we subsume the α/α'-interface contribution into the contribution from α', i.e., we treat the SRO parameter of the α' phase as if it were dependent on the size of the precipitates. This assumption greatly simplified the following treatment and the SRO parameter averaged over the entire sample can be expressed as follows:

$$\langle\beta\rangle = \phi^{\alpha}\beta^{\alpha}[c_{\mathrm{Cr}}^{\mathrm{tot}}] + (1-\phi^{\alpha})\beta^{\alpha'}[c_{\mathrm{Cr}}^{\mathrm{tot}}], \tag{5}$$

where $c_{\mathrm{Cr}}^{\mathrm{tot}}$ denotes the total concentration of Cr in the system and β^{j} is the SRO parameter for the Cr atoms belonging to the α or the α' phase, respectively. The fraction of Cr atoms in the α phase ϕ^{α} can be derived, as shown in the Appendix.

According to Eq. (5) below the solubility limit $\langle\beta\rangle$ equals the SRO parameter of the α phase, the concentration and temperature dependence of which have been discussed in Sec. IV B.

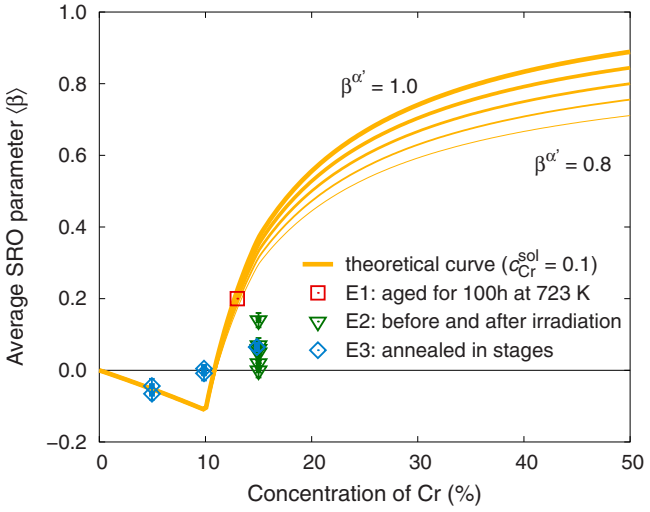

FIG. 7. (Color online) Theoretical prediction for the average SRO parameter $\langle\beta\rangle$ as given by Eq. (5) using Eq. (2) to express the concentration dependence of the SRO parameter in the α phase. Experimental references as given in the caption of Fig. 2. The set of lines between $\beta^{\alpha'}=0.8$ and $\beta^{\alpha'}=1.0$ correspond to different values of $\beta^{\alpha'}$ schematically indicating the effect of coarsening of the α' precipitates.

We now need to discuss the terms in the equation for $\langle\beta\rangle$ which determine the average SRO parameter inside the miscibility gap: The thermodynamic boundary conditions require the Cr concentration in the α phase to be equal to the solubility of Cr in Fe and reciprocally for the α' phase. Due to these constraints, the proportions of α and α' depend only on the total Cr concentration (compare Appendix). Furthermore, since the empirical potential[30] used in this study underestimates the solubility of Fe in Cr, the α' precipitates contain nearly 100% Cr. The solubility also affects the SRO parameter for the α' phase since it correlates with the ratio $Z^{(k)}_{\mathrm{Fe}}/Z^{\mathrm{tot}}_{(k)}$. However, for Fe-rich conditions, this can be safely neglected—again—because of the small solubility. This conclusion is in line with the observations described in Sec. IV C.

In Eq. (5), we have subsumed the contribution of the α/α' interface into $\beta^{\alpha'}$. As shown for example in Figs. 5 and 6(b), the SRO parameter for Cr atoms at the interface is significantly smaller than for atoms in the interior. Therefore, both $\beta^{\alpha'}$ and $\langle\beta\rangle$ depend on the surface to volume ratio of the precipitates. The maximum value for $\beta^{\alpha'}$ is obtained for the limit of a completely coarsened system for which the contribution of the α/α' interface is practically zero ($\beta^{\alpha'}\approx 1$). At the onset of precipitation, the size of the α' precipitates is, however, small and the surface to volume ratio is large. The effective $\beta^{\alpha'}$ is therefore reduced with respect to the fully decomposed system ($\beta^{\alpha'}\approx 0.8$). Hence, depending on the kinetics of the system $\beta^{\alpha'}$ and $\langle\beta\rangle$ can assume a range of values. Both are expected to grow gradually as the system coarsens and gets closer and closer to equilibrium. This is illustrated in Fig. 7 as described in the following.

If one uses the theoretical lower limit for β^{α}, which as shown in Fig. 2 represents the low temperature limit of the simulation data for the α phase, one obtains an entirely analytic expression for $\langle\beta\rangle$. The resulting curves for different values of $\beta^{\alpha'}$ are shown in Fig. 7 where the solubility of Cr has been set to $c^{\mathrm{sol}}_{\mathrm{Cr}}=10\%$ roughly corresponding to the experimental solubility at this temperature. All curves are negative for small Cr concentrations, then pass through zero and eventually approach saturation. The transition from negative to positive values is the hallmark of Cr precipitation and is rather sharp. As discussed above at a given temperature, the only variable is the SRO parameter for the α' precipitates which depends on their size distribution. The most extremal value is $\beta^{\alpha'}=1$ which is achieved if the number of α/α' interface atoms is negligible with respect to the number of atoms in α' precipitates. The resulting curve is shown by the uppermost line in Fig. 7. For smaller α' precipitates, the SRO parameter $\beta^{\alpha'}$ is smaller than 1. The resulting SRO parameter $\langle\beta\rangle$ is shown in Fig. 7 for several values between $\beta^{\alpha'}=0.8$ and 0.95. Upon aging, the average SRO parameter at a given concentration and temperature thus will gradually grow from the lower to the upper curves in Fig. 7. It is apparent from the figure that the effect of a reduced $\beta^{\alpha'}$ becomes notable for $c^{\mathrm{tot}}_{\mathrm{Cr}}\gtrsim 0.2$.

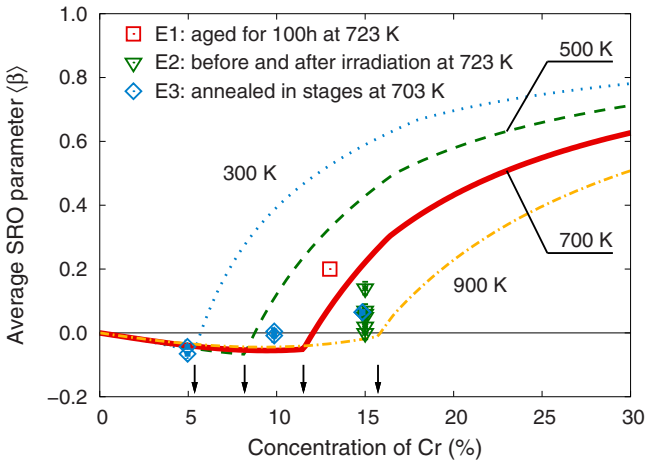

FIG. 8. (Color online) Theoretical prediction for the average SRO parameter based on Eq. (5) using $\beta^{\alpha'}=0.9$ and the simulation data from Fig. 2 for the SRO parameter in the α phase. The temperature dependence of the solubility was taken from Ref. 19 and is indicated by the small arrows at the bottom of the figure.

It should be stressed that the interpretation of the evolution of the average SRO parameter $\langle\beta\rangle$ upon aging is solely based on a gradual approach to equilibrium, i.e., the coarsening of the precipitates. This conclusion is independent of our MC simulations.

B. Comparison to experiments

On the basis of the foregoing analysis, it is now possible to carry out a quantitative comparison with the experimental data points included in Figs. 2, 7, and 8. Since all experiments considered here correspond to temperatures close to 700 K, we focus on the SRO curve calculated at this temperature.

The experimental data point obtained at 5% Cr corresponds to an Fe-rich homogeneous solid solution and the simulation data for the α phase (Fig. 2) as well as the predicted average SRO parameter $\langle\beta\rangle$ (Fig. 7) are in very good agreement.

We suggest that at 10% Cr α' precipitates are formed in the experimental samples which drive the SRO parameter upward leading to an average SRO parameter value close to zero. This trend is reproduced by the theoretical curve which yields a transition through zero close to the experimental data point. The comparison to the calculated curves shows that the inversion of the SRO is very steep and is shifted to slightly larger concentration with respect to the solubility limit.

There are several data points at concentrations close to 15% which are scattered between $\langle\beta\rangle=0.0$ and 0.2: The measurements in Ref. 21 (E1 in Fig. 8) were carried out on a sample aged for 100 hours at 723 K yielding the largest value for the SRO parameter among the experimental data points. The sample measured in Ref. 8 (E3 in Fig. 8) was subjected to isochronal annealing steps at 703 K. In Ref. 22 (E2 in Fig. 8), the authors carried out measurements on different samples before and after irradiation. All samples were initially quenched from 1473 K and subsequently annealed and/or irradiated at 723 K. Irradiation experiments were carried out using both Ar^+ and Fe^+ ions and exposure times ranging from 3 to 30 min. Within the experimental error bars, the SRO parameter was zero for the initial sample. It was observed to increase with exposure time in a series of bombardments with Fe^+. The largest SRO was obtained after extended irradiation with Ar^+ ions.

Collecting the experimental data and using the above analysis, the following interpretation for the observations at higher Cr concentrations emerges: (1) The samples initially obtained by quenching from high temperature show a very small SRO parameter close to zero. This suggests that during rapid quenching from elevated temperatures both the ordering tendency and more importantly the precipitation and growth of α' precipitates are suppressed (lowest data point from E2). (2) On the other hand, the most extensively aged samples show a rather large SRO parameter which is close to the values predicted by the theoretical analysis presented above (E1). This suggests that the α' precipitates in these samples have already reached rather large dimensions (diminishing the contribution of the α/α' interface). (3) Samples subjected to energetic ion beams showed an increase of the average SRO parameter with the intensity of the irradiation, reflecting radiation induced precipitation.

C. Temperature dependence

The shape of the SRO curves and the transition through zero are affected by temperature because of the T dependence of both the SRO in the α phase (Fig. 2) and the solubility of Cr in α-Fe.[19] If these effects are taken into account, one obtains the curves shown in Fig. 8. The increase of the solubility with temperature[19] shifts the transition of the SRO parameter through zero to larger concentrations, whereas the T dependence of the SRO in the α phase (Fig. 2) causes a slight upward shift of the average SRO. Note that the transition through zero is correlated with but not identical to the solubility of Cr.

VI. CONCLUSIONS

In this paper, we have investigated the SRO in Fe-rich Fe-Cr alloys using atomistic simulations based on an empirical potential description of the alloy. For low temperatures and small concentrations the SRO in the α phase is found to be close to the theoretical maximum possible SRO. As temperature increases SRO is reduced due to entropic effects. For somewhat larger Cr concentrations, the SRO curves go through a minimum, which occurs close to the solubility limit. The occurrence of a minimum reflects the competition between energy induced ordering and entropy-driven randomization. It is, however, important to stress that directly at the solubility the SRO is still rather strong.

In the two-phase region, the experimentally measured SRO parameter is a mixture of both the SRO in the α phase and the α' precipitates. The MC simulations show that the two contributions can be clearly separated. When using a weighted average of these contributions the average SRO parameter is predicted as a function of concentration in good agreement with experiment. The MC simulations in conjunction with this simple model demonstrate that the inversion of the SRO parameter experimentally observed is a result of the formation of stable (supercritical) α' precipitates. It is *not* related to the loss of SRO in the α phase, since directly at the solubility limit there is still an appreciable degree of SRO. The model has also been used to investigate the effect of temperature on the SRO parameter which shows the temperature dependence of the solubility of Cr in Fe to be the dominating factor.

The results reported here are anticipated to support future research in at least two aspects: (1) As indicated in the Introduction the SRO affects the mobility of dislocations. The present paper therefore constitutes a basis for a detailed atomistic study of the mobility of dislocations in Fe-Cr alloys following a strategy similar to Ref. 31. (2) The present paper clarifies the contributions to the average SRO parameter in a two-phase system and introduces a simple predictive model. It thereby provides a better understanding of previous experimental results and provides the basis for a more elaborate interpretation of future experiments.

ACKNOWLEDGMENTS

This work was performed under the auspices of the U.S. Department of Energy by the University of California, Lawrence Livermore National Laboratory under Contract No. DE-AC52-07NA27344 with support from the Laboratory Directed Research and Development Program. Generous grants of computer time through the National Energy Research Scientific Computing Center at Lawrence Berkeley National Laboratory are gratefully acknowledged.

APPENDIX

The total number of Fe/Cr atoms is simply the sum of the number of Fe/Cr atoms in the α phase and the α' precipitates,

$$N_{\mathrm{Fe}}^{\mathrm{tot}} = N_{\mathrm{Fe}}^{\alpha} + N_{\mathrm{Fe}}^{\alpha'} \quad \text{and} \quad N_{\mathrm{Cr}}^{\mathrm{tot}} = N_{\mathrm{Cr}}^{\alpha} + N_{\mathrm{Cr}}^{\alpha'}. \tag{A1}$$

In equilibrium, the concentration of Cr in the Fe matrix is given the maximum solubility $c_{\mathrm{Cr}}^{\mathrm{sol}}$. It can be expressed by the number of Fe and Cr atoms in the Fe-rich solid solution $c_{\mathrm{Cr}}^{\mathrm{sol}} = N_{\mathrm{Cr}}^{\alpha}/(N_{\mathrm{Fe}}^{\alpha} + N_{\mathrm{Cr}}^{\alpha})$, which can be rearranged to give

$$N_{\mathrm{Cr}}^{\alpha} = x_{\mathrm{Cr}}^{\mathrm{sol}} N_{\mathrm{Fe}}^{\alpha} \quad \text{with } x_i^j = c_i^j/(1 - c_i^j). \tag{A2}$$

Similarly, the number of Fe atoms in the α' precipitates is connected to the equilibrium solubility of Fe in Cr

$$N_{\mathrm{Fe}}^{\alpha'} = x_{\mathrm{Fe}}^{\mathrm{sol}} N_{\mathrm{Cr}}^{\alpha'}. \tag{A3}$$

Combining Eqs. (A1)–(A3), one obtains

$$N_{\mathrm{Cr}}^{\alpha} = x_{\mathrm{Cr}}^{\mathrm{sol}}(N_{\mathrm{Fe}}^{\mathrm{tot}} - N_{\mathrm{Fe}}^{\alpha'}) = x_{\mathrm{Cr}}^{\mathrm{sol}}(N_{\mathrm{Fe}}^{\mathrm{tot}} - x_{\mathrm{Fe}}^{\mathrm{sol}} N_{\mathrm{Cr}}^{\alpha'}). \tag{A4}$$

Using $N_{\mathrm{Fe}}^{\mathrm{tot}} = x_{\mathrm{Cr}}^{\mathrm{tot}} N_{\mathrm{Cr}}^{\mathrm{tot}}$ and rearranging finally yields

$$\frac{N_{\mathrm{Cr}}^{\alpha}}{N_{\mathrm{Cr}}^{\mathrm{tot}}} = \frac{1/x_{\mathrm{Cr}}^{\mathrm{tot}} - x_{\mathrm{Fe}}^{\mathrm{sol}}}{1/x_{\mathrm{Cr}}^{\mathrm{sol}} - x_{\mathrm{Fe}}^{\mathrm{sol}}} = \phi^{\alpha}. \tag{A5}$$

This expression gives the fraction of Cr atoms in the α phase as a function of the total Cr concentration within the miscibility gap. For Cr concentrations below $c_{\mathrm{Cr}}^{\mathrm{sol}}$ (above $c_{\mathrm{Fe}}^{\mathrm{sol}}$) ϕ^{α} is 1 (0). In summary, ϕ_{α} can be written as

$$\phi^{\alpha} = \begin{cases} 1, & c_{\mathrm{Cr}}^{\mathrm{tot}} < c_{\mathrm{Cr}}^{\mathrm{sol}}, \\ \dfrac{1/x_{\mathrm{Cr}}^{\mathrm{tot}} - x_{\mathrm{Fe}}^{\mathrm{sol}}}{1/x_{\mathrm{Cr}}^{\mathrm{sol}} - x_{\mathrm{Fe}}^{\mathrm{sol}}}, & c_{\mathrm{Cr}}^{\mathrm{sol}} < c_{\mathrm{Cr}}^{\mathrm{tot}} < c_{\mathrm{Fe}}^{\mathrm{sol}}, \\ 0, & c_{\mathrm{Cr}}^{\mathrm{tot}} > c_{\mathrm{Fe}}^{\mathrm{sol}}. \end{cases} \tag{A6}$$

*erhart1@llnl.gov

[1] F. A. Garner, M. B. Toloczko, and B. H. Sence, J. Nucl. Mater. **276**, 123 (2000).
[2] A. Hishinuma, A. Kohyama, R. L. Klueh, D. S. Gelles, W. Dietz, and K. Ehrlich, J. Nucl. Mater. **258-263**, 193 (1998).
[3] N. Saunders and A. P. Miodownik, in *CALPHAD: Calculation of Phase Diagrams*, Pergamon Materials Series Vol. 1, edited by R. W. Cahn (Elsevier Science, Oxford, 1998).
[4] A. T. Dinsdale, CALPHAD: Comput. Coupling Phase Diagrams Thermochem. **15**, 317 (1991).
[5] H. Kuwano and Y. Hamaguchi, J. Nucl. Mater. **155**, 1071 (1988).
[6] V. V. Sagaradze, I. I. Kositsyna, V. L. Arbuzov, V. A. Shabashov, and Y. I. Filippov, Phys. Met. Metallogr. **92**, 508 (2001).
[7] V. A. Shabashov, A. L. Nikolaev, A. G. Mukoseev, V. V. Sagaradze, and N. P. Filippova, Sb. Russ. Acad. Sci. **65**, 1094 (2001).
[8] I. Mirebeau, M. Hennion, and G. Parette, Phys. Rev. Lett. **53**, 687 (1984).
[9] E. Rodary, D. Rodney, L. Proville, Y. Brechet, and G. Martin, Phys. Rev. B **70**, 054111 (2004).
[10] R. L. Klueh and D. R. Harries, *High-Chromium Ferritic and Martensic Steels for Nuclear Applications* (ASTM, West Conshohocken, PA, 2001).
[11] M. Hennion, J. Phys. F: Met. Phys. **13**, 2351 (1983).
[12] P. Olsson, I. A. Abrikosov, and J. Wallenius, Phys. Rev. B **73**, 104416 (2006).
[13] A. A. Mirzoev, M. M. Yalalov, and D. A. Mirzaev, Phys. Met. Metallogr. **97**, 336 (2004).
[14] T. P. C. Klaver, R. Drautz, and M. W. Finnis, Phys. Rev. B **74**, 094435 (2006).
[15] P. Erhart, B. Sadigh, and A. Caro, Appl. Phys. Lett. **92**, 141904 (2008).
[16] P. Olsson, J. Wallenius, C. Domain, K. Nordlund, and L. Malerba, Phys. Rev. B **72**, 214119 (2005).
[17] A. Caro, D. A. Crowson, and M. Caro, Phys. Rev. Lett. **95**, 075702 (2005).
[18] M. Y. Lavrentiev, R. Drautz, D. Nguyen-Manh, T. P. C. Klaver, and S. L. Dudarev, Phys. Rev. B **75**, 014208 (2007).
[19] A. Caro, M. Caro, E. M. Lopasso, and D. A. Crowson, Appl. Phys. Lett. **89**, 121902 (2006).
[20] J. M. Cowley, Phys. Rev. **77**, 669 (1950).
[21] V. V. Ovchinnikov, N. V. Zvigintsev, V. S. Litvinov, and V. A. Osminkin, Fiz. Met. Metalloved. **42**, 310 (1976).
[22] V. V. Ovchinnikov, B. Y. Goloborodsky, N. V. Gushchina, V. A. Semionkin, and E. Wieser, Appl. Phys. A: Mater. Sci. Process. **83**, 83 (2006).
[23] B. Sadigh, P. Erhart, E. Martinez, A. Caro, and L. Zepeda-Ruiz (unpublished).
[24] M. I. Mendelev, S. Han, D. J. Srolovitz, G. J. Ackland, D. Y. Sun, and M. Asta, Philos. Mag. **83**, 3977 (2003).
[25] J. Wallenius, P. Olsson, C. Lagerstedt, N. Sandberg, R. Chakarova, and V. Pontikis, Phys. Rev. B **69**, 094103 (2004).
[26] D. A. Porter and K. E. Easterling, *Phase Transformations in Metals and Alloys* (CRC, Boca Raton, FL, 1992).
[27] A. Caro, M. Caro, P. Klaver, B. Sadigh, E. M. Lopasso, and S. G. Srinivasan, JOM **59**, 52 (2007).
[28] Some data points were directly extracted from figures in the original references by using the software G3DATA (Ref. 29).
[29] J. Frantz (http://www.frantz.fi/software/g3data.php).
[30] The potential used in the present study has been parametrized to exactly reproduce the mixing enthalpy obtained from 0 K DFT calculations (Ref. 12). The mixing curve was calculated with respect to the 0 K reference states (ferromagnetic Fe and antiferromagnetic Cr). Since the real system undergoes several temperature driven transitions, the reference states change and the accordingly the mixing enthalpy. At present this change is, however, not captured by the potential, which causes an underestimation of the solubility of Fe in the α' phase at elevated temperatures. This shortcoming does, however, not affect the main conclusions of the present work.
[31] J. Marian and A. Caro, Phys. Rev. B **74**, 024113 (2006).